Kinetic modelling of runaway-electron dynamics

A Stahl[1], O Embréus[1], E Hirvijoki[1], G Papp[2], M Landreman[3], I Pusztai[1] and T Fülöp[1]

[1] Department of Applied Physics, Chalmers University of Technology, Göteborg, Sweden

[2] Max Planck Institute for Plasma Physics, Garching, Germany

[3] University of Maryland, College Park, MD, USA

E-mail: stahla@chalmers.se

Abstract. Improved understanding of runaway-electron formation and decay processes are of prime interest for the safe operation of large tokamaks, and their dynamics during dynamical scenarios such as disruptions are of particular concern. In this contribution, we present kinetic modelling of scenarios with time-dependent plasma parameters – in particular, we investigate hot-tail runaway generation during a rapid drop in plasma temperature. With the goal of studying runaway-electron generation with a self-consistent electric field-evolution, we also discuss the implementation of a conservative collision operator and demonstrate its properties. An operator for avalanche runaway-electron generation which includes the proper energy dependence of the runaway distribution, is investigated, and the avalanche growth rate is shown to be significantly affected in some parameter regimes. These developments all pave the way for an improved modelling of runaway-electron dynamics during disruptions or other dynamic events.

1. Introduction

In the quest for avoidance or mitigation of the harmful effects of runaway-electron formation [1], a greater understanding of the runaway-electron phenomenon is required. Improved knowledge of runaway-electron formation mechanisms and their dynamics and characteristics will benefit the fusion community and contribute to a stable and reliable operation of reactor-scale tokamaks.

Kinetic simulation is the most accurate and useful method for investigating runaway-electron dynamics, and we recently developed a new tool called CODE (COllisional Distribution of Electrons [2]) for fast and detailed study of these processes. CODE solves the spatially homogeneous kinetic equation in 2-D momentum space, including electric-field acceleration, collisions, avalanche runaway generation and synchrotron-radiation-reaction losses [2, 3, 4]. In CODE, momentum space is discretized using finite differences in momentum and a Legendre-mode decomposition in pitch-angle cosine, and a (quasi-)steady-state solution can be efficiently obtained through the inversion of a single sparse system (in the absence of an avalanche source).

In this contribution we discuss improvements to the model, which enable us to study the effect of hot-tail runaway generation on the electron distribution (Section 2), which can be the dominant mechanism in rapidly cooling plasmas, as well as an improved model for the knock-on collisions leading to avalanche multiplication of the runaway population (Section 4). This model takes the energy dependence of the runaway distribution into account. We also discuss the implementation of a full linearized collision operator, and demonstrate its conservation properties (Section 3).

The improvements described in this contribution enable the detailed study of runaway processes in dynamic situations such as disruptions, and the conservative collision operator makes self-consistent calculations of the runaway population and current evolution in such scenarios feasible [5].

2. Time-dependent plasma parameters

To be able to investigate the behavior of the electron population in dynamic scenarios such as disruptions or sawtooth crashes, it is necessary to follow the distribution function as the plasma parameters change. To this end, CODE has been modified to handle time-dependent background plasma parameters. Since the kinetic equation is treated in linearized form, the actual temperature and density of the distribution are determined by the background Maxwellian used in the formulation of the collision operator. This allows for a scheme where the kinetic equation is normalized to a *reference* temperature $\tilde{T}$ and number density $\tilde{n}$, so that the discretized equation can be expressed on a fixed *reference grid* in momentum space. (Throughout this paper, we will use a tilde to denote a reference quantity.) By changing the properties of the Maxwellian equilibrium around which the collision operator is linearized, plasma-parameter evolution can be modelled on the reference grid without the need for repeated interpolation of the distribution function to new grids.

Analogously to Ref. [2], the kinetic equation in 2D momentum space for the electron distribution function f experiencing a (parallel) electric field E and collisions can be expressed as

$$\frac{\partial F}{\partial \hat{t}} + \hat{E}\left(\xi\frac{\partial F}{\partial y} + \frac{1-\xi^2}{y}\frac{\partial F}{\partial \xi}\right) = \hat{C}\left\{F\right\} + \hat{S}. \tag{1}$$

Here we have introduced a convenient normalized momentum $y = \gamma v/\tilde{v}_e$ – where $\tilde{v}_e = \sqrt{2\tilde{T}/m}$ is the reference electron thermal speed – and the cosine of the pitch angle $\xi = y_\parallel/y$. Using $\kappa = m^3\tilde{v}_e^3\pi^{3/2}/\tilde{n}$, we have also defined the distribution function $F = \kappa f$ (normalized so that $F(y=0) = 1$ for a Maxwellian with $T = \tilde{T}$ and $n = \tilde{n}$), time $\hat{t} = \tilde{\nu}_{ee}t$, and electric field $\hat{E} = -eE/m\tilde{v}_e\tilde{\nu}_{ee}$, as well as the normalized operators $\hat{C} = C\,\kappa/\tilde{\nu}_{ee}$ and $\hat{S} = S\kappa/\tilde{\nu}_{ee}$, with $\tilde{\nu}_{ee} = 16\sqrt{\pi}e^4\tilde{n}\ln\tilde{\Lambda}/3m^2\tilde{v}_e^3$ the reference electron thermal collision time, $-e$, m and v the charge, rest mass and speed of the electron, c the speed of light, and γ the relativistic mass factor. C is the Fokker-Planck collision operator and S an operator describing close (large-angle) Coulomb collisions. These operators will be

discussed more thoroughly in Sections 3 and 4, respectively; for now we just state the new formulation of the collision operator employed in Ref. [2]:

$$\hat{C}^{\mathrm{tp}} = c_C \bar{v}_e^3 y^{-2} \left(\frac{\partial}{\partial y} \left[y^2 \Psi \left(\frac{1}{x} \frac{\partial}{\partial y} + \frac{2}{\bar{v}_e^2} \right) F \right] + \frac{c_\xi}{2x} \frac{\partial}{\partial \xi} (1-\xi^2) \frac{\partial F}{\partial \xi} \right). \tag{2}$$

Here, a bar denotes a quantity normalized to its reference value (i.e, $\bar{v}_e = v_e/\tilde{v}_e$), $x = y/\gamma = v/\tilde{v}_e$ is the normalized speed, $c_C = 3\sqrt{\pi}\bar{\nu}_{ee}/4$, $c_\xi = Z_{\mathrm{eff}} + \Phi - \Psi + \bar{v}_e^2 \delta^4 x^2/2$, Z_{eff} is the effective ion charge, $\Phi = \Phi(x/\bar{v}_e)$ and $\Psi = \Psi(x/\bar{v}_e) = \bar{v}_e^2[\Phi - \bar{v}_e^{-1} x \mathrm{d}\Phi/\mathrm{d}(x/\bar{v}_e)]/2x^2$ are the error and Chandrasekhar functions, respectively, and $\delta = \tilde{v}_e/c$ is assumed to be a small parameter.

Changes to the plasma temperature manifest as shifts in the relative magnitude of the various terms in Eq. (2) (through δ and the quantities with a bar), as well as a change in the overall magnitude of the operator, whereas changes in density only have the latter effect. In both cases, the distribution is effectively colliding with (and relaxing towards) a Maxwellian different from the one native to the reference momentum grid. Heat or particles are introduced to (or removed from) the bulk of the distribution when using this scheme, as all changes to plasma parameters are described by changes to the Maxwellian. This provides a powerful way of simulating rapid cooling, for instance associated with a tokamak disruption.

2.1. Hot-tail runaway-electron generation

If the time scale of the initial thermal quench in a disruption event is short enough – comparable to the collision time – the tail of the initial Maxwellian electron distribution will not have time to equilibrate as the plasma cools. The particles in this supra-thermal tail may constitute a powerful source of runaway electrons, should a sufficiently strong electric field develop before they have time to reconnect with the bulk electrons. This process is known as *hot-tail generation*, and can be the dominant source of runaways under certain conditions [6, 7], and has previously been investigated analytically or using computationally expensive Monte-Carlo simulations [7, 8, 9]. Using CODE to model a temperature drop, we may study a wider range of scenarios and verify the validity of the analytical models.

Figure 1a compares the runaway density evolution computed with CODE to analytical formulas derived in Ref. [9], for a typical hot-tail scenario. The calculations followed the prescribed temperature evolution shown in Fig. 1b and the avalanche source was excluded. The collision operator used in Ref. [9] is the non-relativistic limit of Eq. (2), with $c_\xi = 0$ (the distribution is isotropic since there is no electric field, see below). CODE results using both this operator and the full Eq. (2) are plotted in Fig. 1a, with the latter producing $\sim 50\%$ more runaways in total. This difference can likely be explained by the relatively high initial temperature (3 keV) in the scenario considered, in which case the non-relativistic operator is not strictly valid for the highest energy particles. The analytical formulas use different definitions for n_r; the CODE

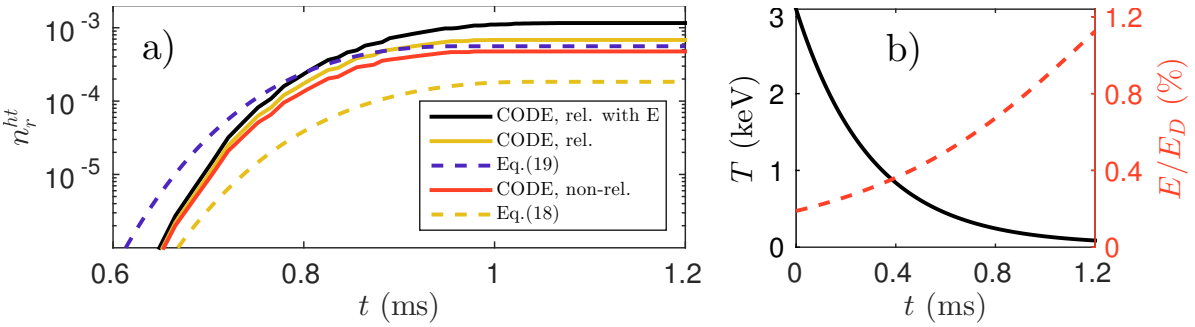

Figure 1. a) Hot-tail runaway density obtained using CODE (solid) – with (black) and without (red, yellow) an electric field included during the temperature drop – and several analytical formulas (dashed), for the temperature and E-field evolution in b). E_D is the Dreicer field and the cited equation numbers refer to Ref. [9].

results are expected to agree with Eq. (19) in Ref. [9], and good agreement is indeed seen for the saturated values in the figure.

The evolution of the temperature and electric-field are shown in Fig. 1b. These are the same as those used in Fig. 5 of Ref. [9], as are all other parameters. The analytical formulas are derived in the absence of an electric field; only an exponential drop in the bulk temperature is assumed. The electric field shown in Fig. 1b is only used to define a runaway region $y > y_c = 1/(\delta\sqrt{E/E_c - 1})$ (with E_c the critical electric field for runaway generation), so that the runaway fraction can be calculated. In other words, it is assumed that the electric field does not have time to influence the distribution significantly during the temperature drop. A CODE calculation where the electric-field evolution is properly included in the kinetic equation is also shown in Fig. 1a (solid black), showing increased runaway production by less than a factor of 2. For the parameters used, the above assumption can thus be considered reasonable.

3. Conservative linearized Fokker-Planck collision operator

Treating the runaway electrons as a small perturbation to a Maxwellian distribution function, the Fokker-Planck operator for electron-electron collisions can be linearized and written as $C\{f\} \simeq C^l\{f,f\} = C^{\mathrm{tp}}\{f_1, f_M\} + C^{\mathrm{fp}}\{f_M, f_1\}$, where f_M denotes a Maxwellian, and $f_1 = f - f_M$ the perturbation to it. The so-called *test-particle term*, C^{tp}, describes the perturbation colliding with the bulk of the plasma, whereas the *field-particle term*, C^{fp}, describes the reaction of the bulk to the perturbation. The full linearized operator C^l conserves particles, momentum and energy. The field-particle term mainly affects the bulk of the plasma, and is therefore commonly neglected when studying runaway-electron kinetics, however the test-particle term alone only ensures the conservation of particles, not momentum or energy.

Under certain circumstances, it is necessary to use a fully conservative treatment also for the runaway problem, in particular when considering processes where the conductivity of the plasma is important. In the study of runaway dynamics during

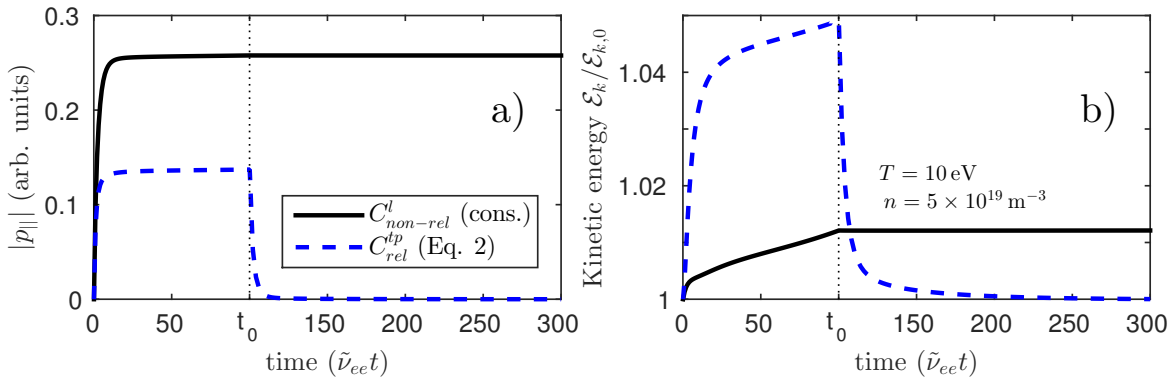

Figure 2. a) Parallel momentum and b) energy moments of the distribution function in CODE, using different collision operators. Initially, $E = 50$ V/m and $Z_{\mathrm{eff}} = 1$ were used, but for $t > t_0$, the electric field was turned off and the ion charge set to $Z_{\mathrm{eff}} = 0$ (to avoid momentum transfer to the background ions). Using two Legendre modes for the field-particle term was sufficient to achieve good conservation.

a tokamak disruption using a self-consistent treatment of the electrical field, accurate plasma current evolution is essential, and the full linearized collision operator must be used. A linearized operator valid for arbitrary particle energy has been formulated [10, 11]. The collision operator originally implemented in CODE is the result of an asymptotic matching between the highly relativistic limit of the test-particle term of that operator with the usual non-relativistic test-particle operator [12], and is given in Eq. (2). The relativistic field-particle term is significantly more complicated, however, and its use would be computationally expensive. Here we instead implemented the non-relativistic field-particle term, as formulated in Ref. [13]. As will be shown, this operator (together with the non-relativistic limit of Eq. 2) accurately reproduces the Spitzer conductivity for temperatures where the bulk is non-relativistic. Using the normalization in Section 2, the operator is

$$\hat{C}^{\mathrm{fp}} = \frac{c_C}{\pi^{3/2}} e^{-\bar{v}_e^{-2}x^2}\left[\frac{2x^2}{\bar{v}_e^4}\frac{\partial^2 G}{\partial x^2} - \frac{2}{\bar{v}_e^2}H + 4\pi F\right], \tag{3}$$

where G and H are the Rosenbluth potentials, obtained from the distribution using

$$\tilde{v}_e^2\nabla_{\mathbf{v}}^2 H = -4\pi F, \qquad \tilde{v}_e^2\nabla_{\mathbf{v}}^2 G = 2H. \tag{4}$$

The system of equations composed of Eqs. (3-4), together with the non-relativistic limits of Eqs. (1-2) ($y \to x$ and $\delta \to 0$), is discretized (see Ref.[2]) and solved using an efficient method described in Ref. [14]. The inclusion of the field-particle term introduces a full block for each Legendre mode into the normally sparse matrix describing the system, however since only a few modes are required to accurately describe the Rosenbluth potentials, the additional computational cost is modest.

The conservation properties of the full non-relativistic collision operator, as well as the relativistic test-particle operator in Eq. (2), are shown in Fig. 2. An electric field was initially used to supply some momentum and energy to the distribution. As expected, the full operator conserves energy and momentum in a pure electron plasma ($Z_{\mathrm{eff}} = 0$)

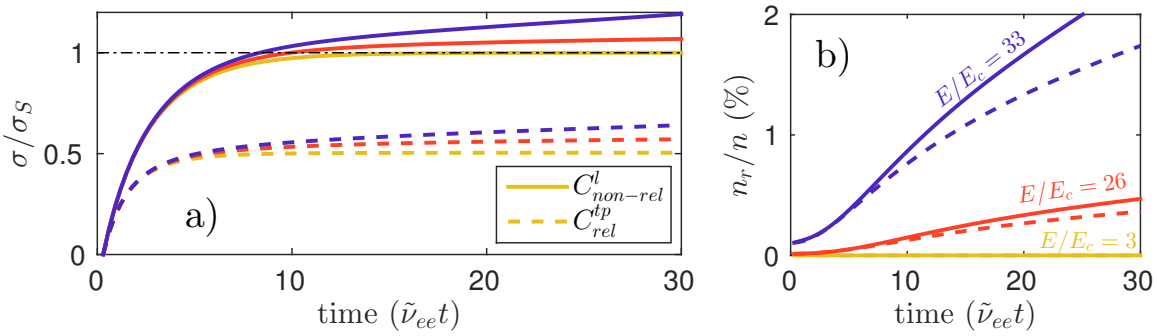

Figure 3. a) Conductivity (normalized to the Spitzer value) and b) runaway density, for different collision operators and E-field strengths, considering only Dreicer runaway generation. The parameters $T = 1$ keV, $n = 5\times10^{19}\,\mathrm{m}^{-3}$ and $Z_{\mathrm{eff}} = 1$ were used.

after the electric field is turned off at $t = t_0 = 100$ collision times, whereas the operator in Eq. (2) does not. The electric field continuously does work on the distribution – a large part of which heats the bulk electron population – but the linearization of the collision operator breaks down if the distribution deviates too far from the equilibrium solution. As long as a non-vanishing electric field is used together with an energy conserving collision operator, an adaptive sink term removing excess heat from the bulk of the distribution must be included in Eq. (1) to guarantee a stable solution. (Physically this accounts for loss processes that are not properly modelled, such as line radiation and radial heat transport.) The magnitude of the black line in Fig. 2b therefore reflects the energy content of the runaway population, not of the total distribution. The sink term is not included for $t > t_0$ (since $E = 0$), and the energy conservation observed is due to the properties of the collision operator itself.

Figure 3 demonstrates that CODE reproduces the expected Spitzer conductivity σ_S for moderate electric field strengths if the conservative collision operator is used, and the initial Maxwellian adapts to the applied electric field on a time scale of roughly 10 collision times. For field strength significantly larger than E_c, the conductivity starts to deviate from σ_S, as a runaway tail begins to form (Fig. 3b); in this regime, the analytical calculation is no longer valid. Using the collision operator in Eq. (2) consistently leads to a lower conductivity (by about a factor of 2), as expected. The runaway growth is also affected, with the conserving operator leading to a larger runaway growth rate.

4. Improved operator for knock-on collision

The Fokker-Planck collision operators discussed in Section 3 accurately describe grazing collisions – small-angle deflections which make up the absolute majority of particle interactions in the plasmas we consider. Large-angle collisions are usually neglected as their cross-section is significantly smaller, but in the presence of runaway electrons they can play an important role in the momentum space dynamics, as an existing runaway can transfer enough momentum to a thermal electron in one collision to render it a

runaway, while still remaining in the runaway region itself. Such *knock-on* collisions can therefore lead to an exponential growth of the runaway density – an *avalanche*.

In the absence of a complete solution to the Boltzmann equation, avalanche runaway generation is modelled using an additional source term in the kinetic equation (1), evaluated for $y > y_c$. A commonly used operator was derived by Rosenbluth and Putvinski [15] and takes the form

$$\hat{S}_{\mathrm{RP}} = \frac{n_r}{n}\,\bar{n}^2 \left[\frac{3\pi\delta^3}{16\ln\tilde{\Lambda}}\delta(\xi-\xi_2)\frac{1}{y^2}\frac{\partial}{\partial y}\left(\frac{1}{1-\sqrt{1+\delta^2y^2}}\right)\right], \tag{5}$$

where n_r is the number density of electrons. In the derivation, the momentum of the incoming particle is assumed to be infinite (and its pitch-angle vanishing), and it is not affected by the interaction. This implies that the generated *secondary* particles are all created on the ellipse $\xi = \xi_2 = \delta y/(1+\sqrt{1+\delta^2y^2})$, and that *all* runaways (from the point of view of the avalanche source) are assumed to have infinite momentum (since $\hat{S}_{\mathrm{RP}} \propto n_r$). They can therefore contribute equally strongly to the avalanche process. This has the peculiar and non-physical consequence that particles can be created with an energy higher than that of any of the existing runaways. The δ-function in ξ is numerically ill-behaved, as it produces significant oscillations (Gibbs phenomenon) when discretized using the Legendre-mode decomposition employed in CODE (see Fig. 4a).

An operator that relaxes the assumption of infinite runaway momentum has been presented by Chiu et al. [16]. It has the form

$$\hat{S}_{Ch}(y,\xi) = \bar{n}\,\frac{2\pi e^4}{m^2c^3}\,\frac{\tilde{n}\delta^3}{\tilde{\nu}_{ee}}\,\frac{x}{y^2\xi}\,(y_{\mathrm{in}})^4\,F^\star(y_{\mathrm{in}})\,\Sigma\left(\gamma,\gamma_{\mathrm{in}}\right), \tag{6}$$

where Σ is the Møller scattering cross-section [17] and $F^\star$ is the pitch-angle-averaged distribution of incoming runaways with properties y_{in} and γ_{in}. All incoming particles are thus still assumed to have zero pitch angle ($\xi = 1$), but their energy distribution is properly taken into account. In CODE, $F^\star$ is efficiently computed from the 0th Legendre mode of F, $F^\star = 2F_0$.

From the conservation of 4-momentum in a collision, the momentum-space coordinates are related through

$$\xi = \sqrt{(\gamma-1)(\gamma_{\mathrm{in}}+1)/(\gamma+1)(\gamma_{\mathrm{in}}-1)}, \tag{7}$$

which restricts the momentum-space region where the source is non-vanishing. Since the electrons participating in a collision are indistinguishable, it is sufficient to consider only the cases where the energy of the created secondary runaway is less than half of the primary energy, $(\gamma-1) \leq (\gamma_{\mathrm{in}}-1)/2$, which leads to the condition $\xi \leq \xi_{\max} = \sqrt{\gamma/(\gamma+1)}$. By the same argument, the maximum attainable runaway energy in the simulation (the maximum of the momentum grid) leads to the condition $\xi \geq \xi_{\min} = \sqrt{(\gamma-1)(\gamma_{\max}+1)/(\gamma+1)(\gamma_{\max}-1)}$.

The magnitudes of the two sources (5) and (6) are computed from a given typical runaway distribution function, and shown in Fig. 4a and b. Note that the amount of numerical noise is significantly reduced for the source in Eq. (6). Fig. 4c shows the source magnitudes integrated over pitch-angle, and as expected, the source in Eq. (6)

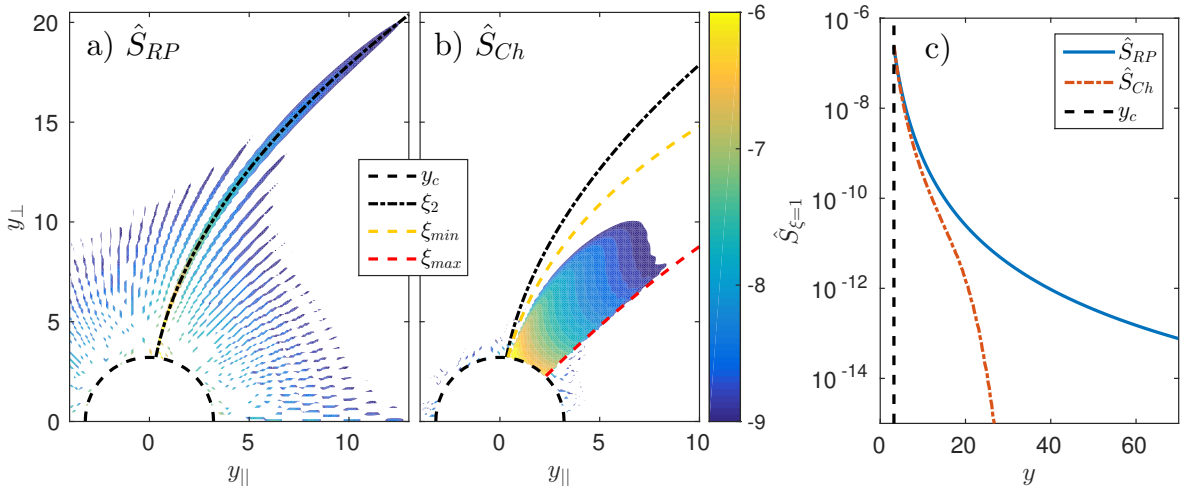

Figure 4. Contour plots of the magnitude of the source in a) Eq. (5) and b) Eq. (6) in $(y_\parallel, y_\perp)$ momentum space, given the same electron distribution. The plotted quantity is $\log_{10}\hat{S}$ and y_c defines the lower bound of the runaway region. The angle-averaged source magnitudes are shown in c). The parameters $T = 1$ keV, $n = 5 \times 10^{19}$ m^{-3}, $Z_{\text{eff}} = 1$ and $E = 1$ V/m were used, with $\max(y) = 70$, and the simulation was run for 300 collision times with primary generation only.

extends only up to $y \simeq y_{\max}/2$, whereas the source in Eq. (5) is non-vanishing also for larger momenta. The amount of secondary runaways generated by the two sources agree well at low energies, but less so further away from the bulk. The total source magnitude $\int \hat{S} \mathrm{d}y\mathrm{d}\xi$ is however similar, since most of the secondaries are created close to the boundary of the runaway region.

Such good agreement is not always observed, however. Figure 5 compares the total runaway growth rate (Dreicer+avalanche) using the two sources, for several different parameter sets (with Fig. 5b corresponding to the parameters used in Fig. 4). The figure shows that the sources can lead to significantly different growth rates. In Fig. 5a (high T, relatively weak E field) the Rosenbluth-Putvinski source gives a higher growth rate, whereas the situation is reversed in Fig. 5c (low T, relatively weak E field). In the intermediate case in Fig. 5b, the growth rate is similar for the two sources.

It is evident that the improved avalanche operator in Eq. (6) can affect the runaway dynamics significantly compared to the operator in Eq. (5) – at least in certain parameter regimes – and may lead to more accurate modelling of runaway avalanches. Together with the ability to model dynamic scenarios and the possibility to allow for self-consistent calculation of the plasma current, the work presented here can therefore lead to a better assessment of the risks posed by runaways in future tokamaks such as ITER.

5. Conclusions

In this contribution we have described several improvements to the numerical tool CODE, used for calculating the momentum space distribution of runaway electrons.

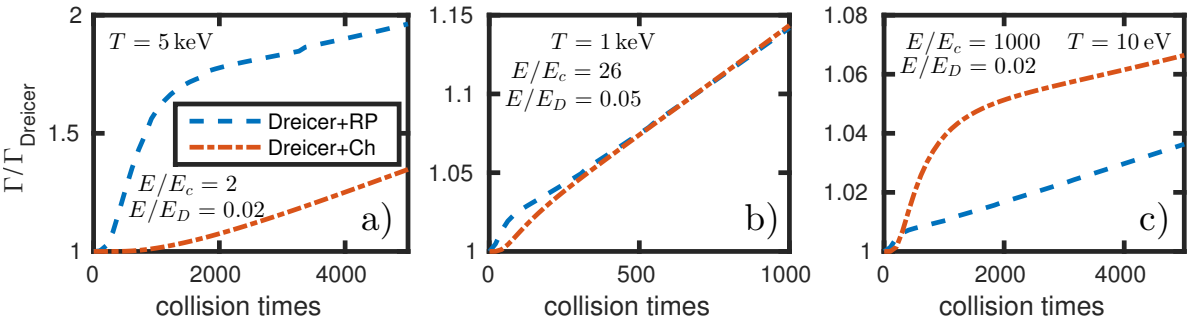

Figure 5. Runaway growth rate (normalized to the Dreicer growth rate) in CODE simulations using the avalanche operators in Eq. (5) (RP, dashed) and Eq. (6) (Ch, dash-dotted), for various temperatures and E fields. The parameters $n = 5 \times 10^{19}\,\mathrm{m}^{-3}$ and $Z_{\mathrm{eff}} = 1$ where used.

We have adapted CODE to be able to account for time-varying plasma parameters, and have used it to study rapid-cooling scenarios where hot-tail runaway-electron generation is dominant. Good agreement with previous theoretical work was observed. Furthermore, an implementation of the full, linearized, non-relativistic collision operator was described, showing excellent conservation properties and reproducing the expected Spitzer conductivity in the relevant parameter regime. An improved operator for close Coulomb collisions, relaxing some of the approximations of the commonly used Rosenbluth-Putvinski operator, was also discussed. It was found that the avalanche growth rate can be significantly effected – either increased or decreased, depending on the parameter regime – by the use of the new operator. The work presented here paves the way for more accurate modelling of runaway electron dynamics during for instance tokamak disruptions.

References

[1] E. M. Hollmann, et al., Phys. Plasmas **22**, 021802 (2015).
[2] M. Landreman, A. Stahl and T. Fülöp, Comp. Phys. Comm. **185**, 847 (2014).
[3] A. Stahl, E. Hirvijoki, J. Decker, O. Embréus and T. Fülöp, Phys. Rev. Lett. **114**, 115002 (2015).
[4] E. Hirvijoki, et al., J. Plasma Phys. **81**, 475810502 (2015).
[5] G. Papp, et al., European Conference Abstracts **39E**, P1.173 (2015).
[6] R. W. Harvey, et al., Phys. Plasmas **7**, 4590 (2000).
[7] P. Helander, H. Smith, T. Fülöp and L.-G. Eriksson, Phys. Plasmas **11**, 5704 (2004).
[8] H. Smith, P. Helander, L.-G. Eriksson and T. Fülöp, Phys. Plasmas **12**, 122505 (2005).
[9] H. M. Smith and E. Verwichte, Phys. Plasmas **15**, 072502 (2008).
[10] S. T. Beliaev and G. I. Budker, Sov. Phys. Dokl. **1**, 218 (1956).
[11] B. J. Braams and C. F. F. Karney, Phys. Fluids B **1**, 1355 (1989).
[12] G. Papp, M. Drevlak, T. Fülöp and P. Helander, Nucl. Fusion **51**, 043004 (2011).
[13] B. Li and D. R. Ernst, Phys. Rev. Lett. **106**, 195002 (2011).
[14] M. Landreman and D. R. Ernst, J. Comput. Phys. **243**, 130 (2013).
[15] M. N. Rosenbluth and S. V. Putvinski, Nucl. Fusion **37**, 1355 (1997).
[16] S. C. Chiu, M. N. Rosenbluth, R. W. Harvey and V. S. Chan, Nucl. Fusion **38**, 1711 (1998).
[17] C. Møller, Ann. Phys. **406**, 531 (1932).